

# Morphological Evolution of Andesite Railway Ballast Particle Under Rotating Drum Abrasion Test



O. C. Debanath, T. Matsushima, T. Ijichi, and M. Miwa

**Abstract** Railway ballast is a natural aggregate widely used in railway infrastructure. The mechanical strength and geometric shape of ballast particles have an important role in the durability and maintenance economy of the ballasted track. This paper aimed to investigate the abrasive behavior of andesite ballast particles using a rotating drum abrasion test and 3D morphological shape analysis. The photogrammetric reconstruction method is adopted here and modified to make it more efficient and user-friendly. The evolution of mass, particle shape, and grain indices were compared for different shape classifications. The experimental results show that the evolution of elongation and flakiness that describe overall particle shape is inconsistent during abrasion, whereas the equivalent ellipsoid volume ratio and rotational resistant angle, which mainly describe particle surface angularity evolve gradually throughout this long-term abrasion process. So, the latter two shape indices describe particle abrasion behavior more accurately.

**Keywords** Railway ballast · Long-term abrasion · Rotating drum test · Photogrammetric reconstruction · Particle shape analysis

---

O. C. Debanath

Doctoral Program in Engineering Mechanics and Energy, University of Tsukuba, Tsukuba, Japan

Department of Civil Engineering, CUET, Chittagong, Bangladesh

T. Matsushima (✉)

Department of Engineering Mechanics and Energy, University of Tsukuba, Tsukuba, Japan

e-mail: [tmatsu@kz.tsukuba.ac.jp](mailto:tmatsu@kz.tsukuba.ac.jp)

T. Ijichi · M. Miwa

JR Central, Nagoya, Japan

e-mail: [takuya.ijichi@jr-central.co.jp](mailto:takuya.ijichi@jr-central.co.jp)

M. Miwa

e-mail: [m.miwa@jr-central.co.jp](mailto:m.miwa@jr-central.co.jp)

## 1 Introduction

Natural stones are the most common type of material with various engineering applications since prehistoric times, specifically for railway lines; crushed stones are the prime element of the ballast layer. Andesite rock is one of the most common igneous rocks used in railway infrastructure. A major concern about rail tracks is the instability of the track, which mainly depends on the geometric stability and settlement of the underlying ballast layer. Moreover, the stability of the ballast layer depends on the interlocking of particles, gradation, particle shape, hardness, and abrasion resistance. The mechanical stability and economic efficiency of railway tracks greatly depend on the rate of ballast degradation (crushing and abrasion) due to the cyclic traffic load throughout its lifecycle.

Several researchers [1–3] investigated ballast particle degradation by laboratory tests such as Los Angeles abrasion, micro-Deval abrasion, direct shear, and large-scale triaxial test. They suggested that the ballast abrasion rate depends on its rock type, physical properties, external loading condition, etc. The grain shape is another important parameter that significantly affects the ballast particle performance. The relationship between the particle shape and abrasion value was reported by previous research [4–6]; typically, the flaky or elongated particles are more susceptible to breaking. The correlation between the mechanical strength and the physical properties of rock material was also studied by previous researchers [5, 7]. Guo [8] proposed a technique based on abrasion depth and 3D sphericity of particles to quantify the degradation. Similar research findings also revealed the relationship between the micro-Deval loss and the angularity of western Virginia aggregate [9].

Considering the durability phenomena, the long-term abrasive behavior is important, which requires some additional tests beyond the standard test methods. Czinder [10] reported that the short-term micro-Deval abrasion test is insufficient to represent the overall abrasion process. A typical andesite rock requires approximately 2 million abrasion cycles for 80% weight loss. In contrast, relatively soft rocks require up to 300,000 cycles, and the abrasion process is reported as a function of mechanical work done following exponential form. A limited number of research studies was done on 3D shape analysis of particle, which only focused on short-term abrasion. However, it is still important to understand ballast particles' long-term abrasion behavior, including morphological changes.

The present study attempts to observe the abrasive behavior of ballast particles using a rotating drum device to look up the in-depth morphological transformation during long-term abrasion by using 3D particle shape analysis. Particle shape is defined by considering flakiness and elongation. There are many conventional shape descriptors to describe the grain shape, such as true sphericity, form factor, shape factor, angularity, texture, etc. In the current research, we introduced two new parameters ellipsoid volume ratio and rotational resistant angle. The evolution of these parameters was then correlated with volumetric degradation of ballast particles along with physical photographs at different abrasion stages for clear visualization of long-term abrasion phenomena.

## 2 Materials and Experimental Workflow

The material used in this study was irregularly shaped andesite ballast particles of about 5 cm. Their average density was about  $2.62 \text{ gm/cm}^3$ . The Photogrammetric reconstruction technique was used to measure the 3D surface morphology of about 50 particles. Among them, nine particles were selected for morphological evolution observation considering the variety of particle shapes. The evolution of particle mass, 3D models, and other shape indices were recorded at various stages of the abrasion process. Details of the experimental setup and workflow are described in the following subsections.

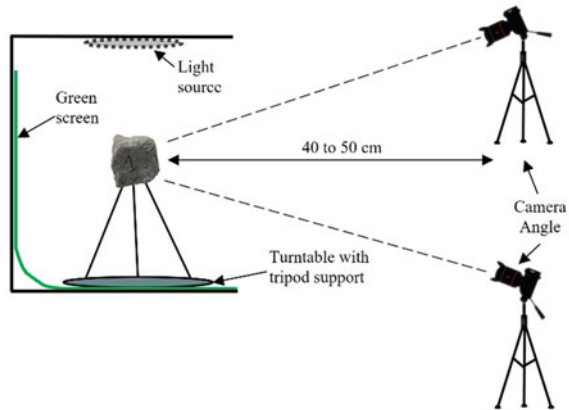
### 2.1 Three-Dimensional Shape Extraction

Recent articles have reported the use of 3D scanning techniques such as laser scanners, X-ray CT scanners, photogrammetric reconstruction, and light-based 3D scanners to extract the three-dimensional shape of ballast particles [11–13]. Laser or X-ray CT scanning is a very popular and primitive technique for digital model reconstruction of any solid object; specifically, laser scanning is an active method of shape reconstruction, where the laser beams reflected from the surface are recorded on the sensor. The suitability of the above-mentioned techniques depends on the object size, shape, surface irregularity, scanning resolution, etc. Several previous researchers used the laser technique to study 3D shapes. For an angular shape ballast particle, it often requires scanning the particle in different orientations and then aligning the meshes by using common surface points to generate the final shape. However, this workflow includes significant time starting from scanning and mesh processing, which is less effective for a large-scale experimental campaign. To overcome this drawback of previous digital reconstruction methods, Paixão [14] introduced the photogrammetry method to make this process more efficient. In this current study, we modified this workflow to make it more user-friendly and time efficient. A detailed description of the workflow is shown in Fig. 1.

For the photographic session, a photographic box was assembled with diffused light source at the top and all the box's inner walls with reflective material to ensure enough light to the object. We used green screen background and a turntable assembled with a tripod needle stand. The tripod stand facilitates the easy placement of particles. In contrast, the previous method [14] needs to drill an orifice at the particle surface to mount on the single pedestal support that may propagate microcracks on the rock surface. The turntable is placed at the center of the assembly and then rotated at a constant speed of 2 rpm. For each particle placed in the turntable, sequential photographs were captured to cover the  $360^\circ$  view at every  $10^\circ$  interval to confirm sufficient overlaps on successive images.

We used a digital camera (Canon EOS Kiss X7 18 MP) equipped with EFS 17–18 mm lens; the camera settings were as follows: manual focus with exposure time 1/

**Fig. 1** Photographic arrangement



400 s., ISO-6400, and aperture F/8. For each 3D model, 72 photographs were captured from two different vertical positions (approximately  $45^\circ$  with horizontal). The overall photographic session took approximately 3 min per particle, from placement on the tripod stand to the end of the photo session. The next part of the reconstruction is done using Agisoft Metashape (student edition) software [15]. The first step is to align photos sequentially, taking the key point limit per MP as 5000; Afterward, the dense cloud is built at moderate depth filtering; Fig. 2 (a) shows the noise-free dense point cloud. In this workflow, no undesired points are generated, which makes the next step (mesh processing) easier, whereas the VisualSFM and CMVS algorithms used by previous authors build numerous background noises in the dense cloud. Moreover, the Agisoft Metashape software facilitates simultaneous data processing of multiple particles, which makes the workflow more efficient. The rest of the part is done by another software, CloudCompare [16], to erase the tripod support from the dense cloud and Screened Poisson mesh reconstruction. The reconstructed meshes need to be scaled correctly to represent the original particle. In the current study, the geometric scale factor is computed by taking the bouncy volume of the particle and applied for uniform scaling in all directions. Figure 2(b–c) represent the final 3D model and original particle, respectively.

In this modified photogrammetric reconstruction workflow, the average reconstruction time taken for each particle is about 10 min, while the method proposed by Paixão [14] takes around one hr. per particle, and other 3D reconstruction techniques are more time-consuming. At the beginning of this experimental campaign, we scanned the same particle using a laser scanner (Roland LPX-60) with 0.2 mm accuracy; after that, both models were overlapped to check the accuracy of photogrammetric reconstruction. Figure 2(d) illustrates the deviation between the laser-scanned and the photo-reconstructed mesh. Both meshes were closely matched, and for most of the vertices, the deviation was observed between  $-0.2$  mm and 0.3 mm, whereas the accuracy of the scanner was 0.2 mm. Moreover, the laser scanner took around 45 min to scan the particle in one orientation. Multiple orientations were needed for a very angular particle, and the laser beams sometimes failed to capture the extreme

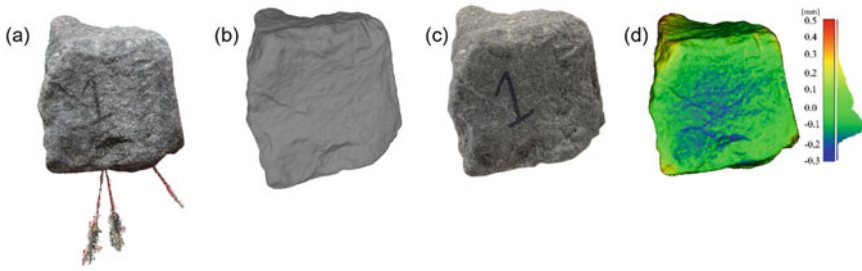


**Fig. 2** a Reconstructed dense cloud b Final 3D mesh c Original Ballast particle d Deviation with laser scanning

concave surface points. Hence the modified photogrammetric reconstruction method was chosen for the rest of this research.

### 2.2 Sample Selection

Around 50 representative particles were scanned by photogrammetric reconstruction, and 3D model has generated afterward. In this study, we used the best-fit ellipsoid concept to determine the dimensions of ballast particles. First, the best-fit ellipsoid was defined such that the three principal moments of inertia are identical to those of the original particle, and the maximum, intermediate, and minimum axes, denoted as  $L$ ,  $I$ , and  $S$ , respectively, were computed from the ellipsoid. Figure 3(a) illustrates the best-fitted ellipsoid over the original particle.

Therefore, elongation ( $I/L$ ) and flakiness ( $S/I$ ) are used to describe the overall shape of the particle. In this study, modified Zingg [17] form terminology was used

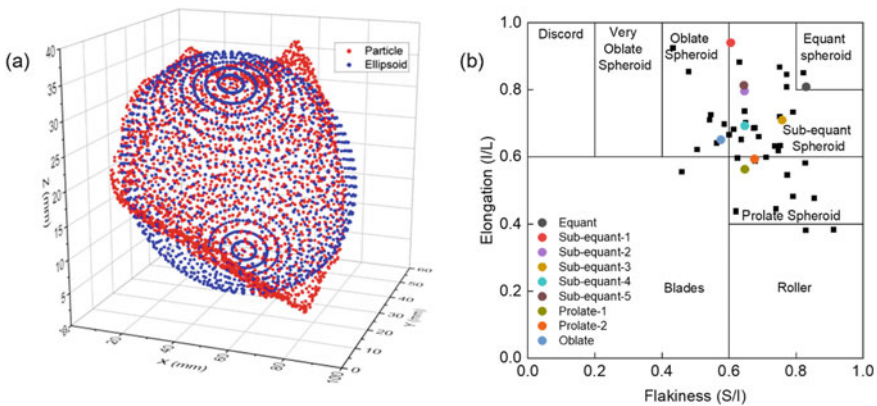


**Fig. 3** a Illustration of Equivalent ellipsoid b Morphological classification of scanned particles

based on the degree of elongation and flatness. Black square dots in Zingg's diagram shows the shape of the measured particles, Fig. 3(b). Among them, five Sub-equant, two prolate, one oblate, and one equant spheroid were chosen for details inspection, marked by colored circles in Zingg's diagram.

### 2.3 Test Setup

We used a modified micro-Deval setup to accelerate the abrasion process, this modification was made based on available laboratory facilities. Figure 4 shows the setup of the test device. The inner diameter of the drum was 30 cm, and an inner shaft of 5 cm width was fixed to let the particle fall from a certain height and collide with the inner wall of the drum during the drum rotation. The rotational speed was kept constant (70 rpm) throughout the test. The test was conducted for an extended abrasion cycle to observe the long-term degradation until the particle mass loss reached 70–90%. The previous studies [18] reported that the rate of abrasion is very high initially and trending to be constant afterward. The experimental program was set to interrupt the abrasion process at irregular intervals; the test data was initially recorded at intervals of 2000, 14,000, and 50,000 rotations, respectively; afterward, approximately fifty thousand rotations intervals until desired weight loss was achieved. The mass of individual particles was recorded at every incremental stage of abrasion, and the 3D shape extraction was done simultaneously for all selected particles. If any particle was broken during this process, the fine fragments were discarded, and the remaining part of the particle was subjected to the next stage.



Fig. 4 Rotary drum abrasion test setup

### 3 Results and Discussions

To describe the grain shape evolution, here we considered two new grain descriptors named: the equivalent ellipsoid volume ratio and rotational resistance angle for shape evolution. As mentioned above, the weight loss and 3D model were recorded at each incremental abrasion stage; then, further analysis was carried out based on the extracted virtual shape to obtain various shape indices. The detailed results are described in the following subsections.

#### 3.1 Particle Mass Evolution

The individual particle mass recorded at the incremental stage of abrasion was used to compute the percentage of mass loss compared to the initial mass of the corresponding particle. Figure 5(a) shows the particle mass change during long-term abrasion; each line of this graph represents individual particle mass evolution. The generated abraded materials were mostly fine dust; few particles were broken at a sudden stage of abrasion, and any representable part from broken particles was also further tested; otherwise, the fine fragments were discarded. For example, the particle sub-equant-5 was broken into fine fragments after 50,000 revolutions, and no representing parts remained; hence that particle was discarded from the analysis. On the other hand, the sub-equant-1 particle was divided into two after 142,000 revolutions; these fragments continued to be abraded and analyzed as two independent particles in the next phase. The sudden increase of particle mass loss is due to the particle breaking event at that phase; the sub-equant-3, prolate-2, and oblate particles were subjected to sudden breaking at several test stages. The physical photographs of particles captured at different test stages also confirmed this.

At the initial phase of abrasion, specifically below 10% mass loss, all the shapes showed a similar abrasion rate, which decreased in the later phase. The angularity of particles can describe this behavior; at the early stage, sharp edges and vertices were broken, resulting in higher mass loss, and reduced afterward. Considering long-term abrasion, the degradation of equant and sub-equant spheroid particles shows analogous behavior. Other shapes like oblate or prolate spheroid undergo high degradation, possibly due to continuous edge breaking.

#### 3.2 Particle Shape Evolution

The typical way of representing the particle shape is based on its flakiness and elongation; as defined earlier, the value of flakiness and elongation is less than 1. Several classification methods are available to describe the particle shape, and the modified Zingg's classification was adopted in our study. Figure 5(b) shows the shape

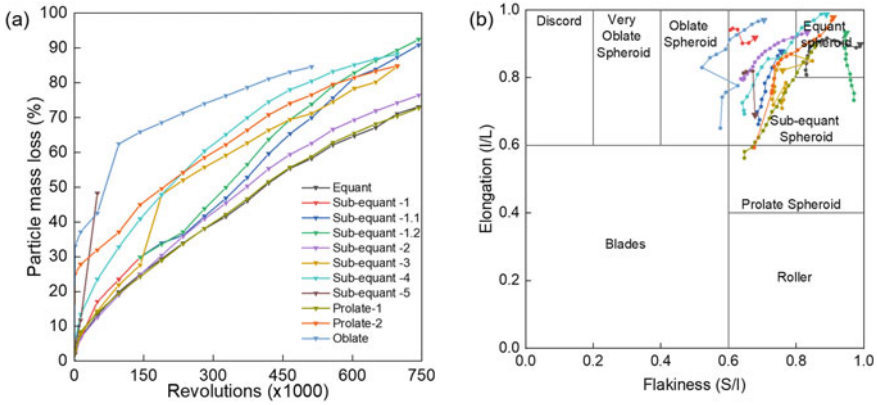


**Fig. 5** Evolution of **a** particle mass and **b** shape movement of studied particles in modified Zingg’s diagram

evolution of nine particles within modified Zingg’s diagram during the abrasion test. The line colors represent the same particle as listed in Fig. 5(a); the circular marker indicates the shape of the particle at different stage of abrasion, whereas the larger circular and triangular markers represent the initial and final shape, respectively.

Significant shape change was recorded during this long-term abrasion process. Figure 6 illustrates the visual change of the studied particles during the test. From visual inspection, it was seen that the sharp edges disappeared quickly, specifically during the first 2000 revolutions. And the smoother shapes appeared afterward due to loss of surface roughness by continuous polishing action inside the drum; this characteristic is reported as rolling erosion of rock [19]. At the initial configuration of the test, we started with the particles of different shape classes. However, at the final stage (after 70–90% loss), all particles’ classified as an equant spheroid shape. It was also noticed that elongation’s evolution was higher than the evolution flakiness. In the conventional micro-Deval abrasion test reported by a previous study [18], no evolution was recorded regarding particle shape classification. But the long-term abrasion test significantly changes the initial form of particle. This shape transformation of the particle during long-term abrasion can be noted as an important finding, as the overall stability of the ballast layer depends on the geometric shape.

### 3.3 Morphological Evolution

Several shape indices were used in previous literature to explain the morphology of angular particles. In this study we considered two overall indices: (i) flakiness, (ii) Elongation; and two detailed morphological indices: (iii) ellipsoid volume ratio, (iv) rotational resistant angle, respectively. The volume change for a homogeneous rock material is equivalent to the particle mass change. Hence, we considered the volume



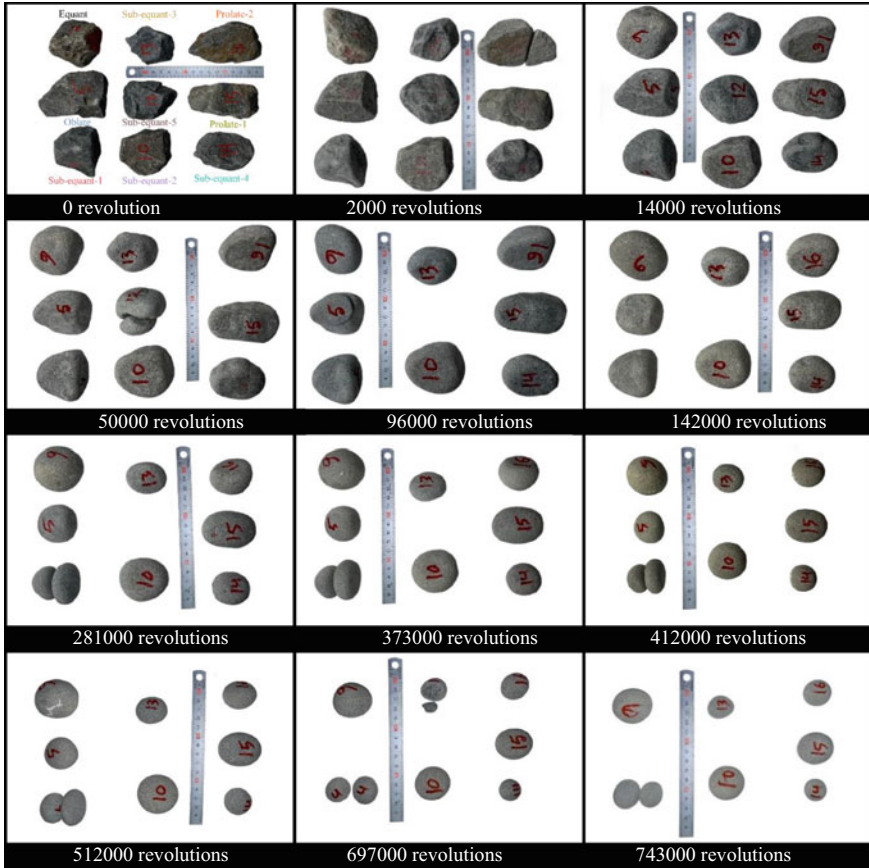
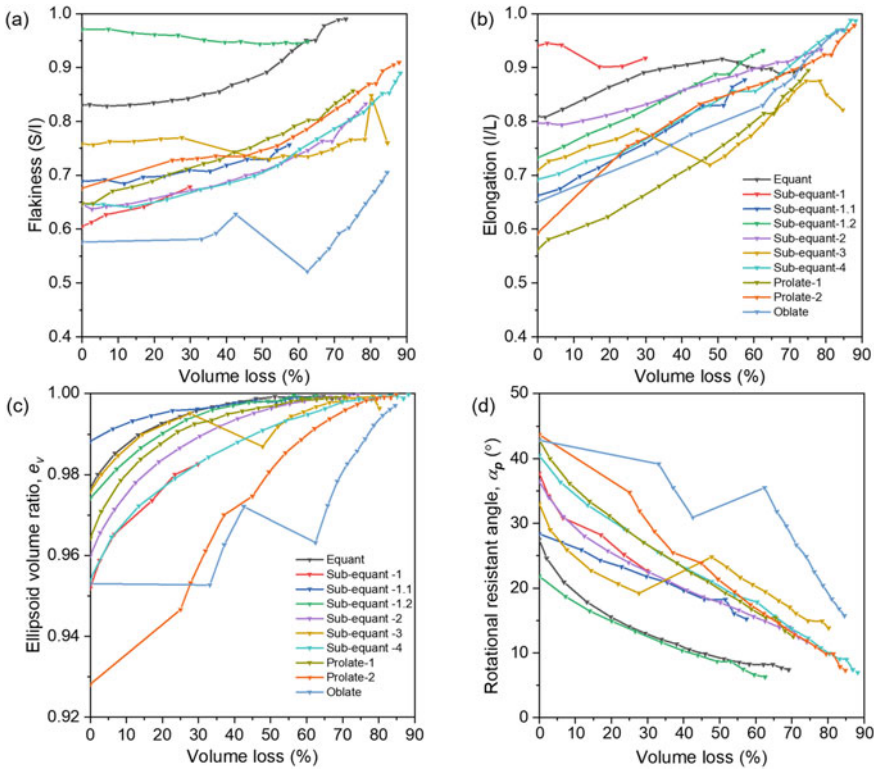


Fig. 6 Changes of particle shape during abrasion test

loss to describe the evolution of these parameters (Fig. 7). Although the particle shape changed significantly, the evolution of flakiness and elongation showed different evolution behavior during this long-term abrasion process. Referring to Fig. 7(a–b), the value of flakiness didn’t change much initially, specifically up to 30% volume loss, and after that, this value increased gradually. In contrast, the evolution of elongation happened constantly and merged in the range of 0.8–1; this evolution trend resulted from nonuniform abrasion of particles in all directions.

As described in Sec 2.2, a best-fit ellipsoid is generated for each 3D particle model such that the three principal moments of inertia are identical to those of the original particle. Figure 3(a) illustrates the best fitted ellipsoid over the original particle. Since the volume of the fitted ellipsoid is different from that of the original particle, and this difference is due to the detailed angularity difference, a shape index called, ellipsoid volume ratio ( $e_v$ ) is defined by the ratio of the original particle volume to the best-fit ellipsoid. The value of the ellipsoid volume ratio is smaller than unity when the



**Fig. 7** Evolution of **a** Flakiness, **b** Elongation, **c** Ellipsoid volume ratio and, **d** Rotational resistant angle

particle shape deviates more from the ellipsoid. Figure 7(c) shows the evolution of the ellipsoid volume ratio; at the initial stage of abrasion, the  $e_v$  value was different for different shapes and typically lies within the range of 0.928–0.98. However, this value moved towards unity for all particles regardless of the shape classification at the final stage of abrasion. This increase of  $e_v$  was due to the continuous polishing effect inside the drum, which resulted in particles close to an ellipsoid shape.

Another shape parameter is a mechanically based shape index, called the rotational resistant angle,  $\alpha_p$  proposed by Kawamoto [20]. For any surface point of 3D mesh,  $\alpha$  is the angle between the surface normal of that point and the radial vector of joining the line of particle centroid, and  $dS$  is the area of the corresponding triangular face. Finally,  $\alpha_p$  is calculated by taking the weighted average  $\alpha$  over the entire surface of the particle as described in Eq. (1); here,  $A$  is the total surface area of the mesh.

$$\alpha_p = \frac{1}{A} \int \alpha \, dS \tag{1}$$

The value of  $\alpha_p$  is linked to the rolling resistance acting on two particles in contact, and it increases with increasing particle surface angularity. Regarding the evolution of  $\alpha_p$ , this parameter varied from 27 to 43 degrees before abrasion; after long-term abrasion, this range was decreased. The Minimum value of  $\alpha_p$  was found for the equant shape ballast at the final configuration. For both cases, the abrupt particle breaking was reflected as a sudden transition of shape index, specifically for sub-equant-3 and oblate spheroid. As the shape indices (S/I and I/L) didn't change consistently throughout the abrasion cycle, the other conventional parameters (such as sphericity, roundness, form factor, etc.) based on overall shape are not a good measure to represent the abrasion. On the other hand, the evolution of detailed shape indices ( $e_v$  and  $\alpha_p$ ) was consistent throughout the long-term abrasion and can describe the abrasion of the local corners. Therefore, the latter two indices can be taken as more suitable parameters to track the abrasive behavior of ballast particles.

## 4 Conclusion

In this paper, the rotating drum test was used to study the morphological evaluation of andesite ballast particles having varying shapes. The test was interrupted at different intervals, and 3D mesh of selected particles was generated by photographic session and 3D reconstruction technique. To observe the effect of accelerated long-term abrasion, the evolution was tracked in terms of weight loss, shape movement, ellipsoid volume ratio, and rotational resistant angle obtained from 3D shape analysis.

The particle mass loss data reveals the high abrasion initially and slower rate afterward, except for some abrupt changes due to fragmentation. Compared to the short-term abrasion test, significant shape change was observed during the long-term abrasion process, where all the particles changed their initial shape classification. The corner breaking and particle fragmentation also occurred throughout the test and were reflected as sudden transitions of mass loss and shape index. The initial ellipsoid volume ratio deviated far from unity and converged significantly because of the rolling action inside the drum. Reasonable change of the shape indices proves the validity of the adopted method. It is suggested that the equivalent ellipsoid volume ratio and rotational resistance angle are good indices compared to overall shape index flakiness and elongation to evaluate the ballast particle abrasion.

Considering the micro-scale morphology, local abrasion parameters such as the local curvature and wear depth are other important parameters that are not analyzed in the current study. However, future study is expected to include these issues to develop an abrasion model that may help to predict ballast particles' abrasive behavior.

## References

1. Wu J, Hou Y, Wang L, Guo M, Meng L, Xiong H (2018) Analysis of coarse aggregate performance based on the modified Micro Deval abrasion test. *Int J Pavement Res Technol* 11:185–194. <https://doi.org/10.1016/j.ijprt.2017.10.007>
2. Sun Y, Zheng C (2017) Breakage and shape analysis of ballast aggregates with different size distributions. *Particuology* 35:84–92. <https://doi.org/10.1016/j.partic.2017.02.004>
3. Qian Y, Tutumluer E, Hashash YMA, Ghaboussi J (2022) Triaxial testing of new and degraded ballast under dry and wet conditions. *Transp Geotech* 34:100744. <https://doi.org/10.1016/j.trgeo.2022.100744>
4. Maroof MA, Mahboubi A, Noorzad A, Safi Y (2020) A new approach to particle shape classification of granular materials. *Transp Geotech* 22:100296. <https://doi.org/10.1016/j.trgeo.2019.100296>
5. Kim J, Park B-S, Woo SI, Choi Y-T (2020) Evaluation of ballasted-track condition based on aggregate-shape characterization. *Constr Build Mater* 232:117082. <https://doi.org/10.1016/j.conbuildmat.2019.117082>
6. Sun Y, Indraratna B, Nimbalkar S (2014) Three-dimensional characterisation of particle size and shape for ballast. *Géotechnique Lett* 4:197–202. <https://doi.org/10.1680/geolett.14.00036>
7. Rangaraju PR, Edlinski J (2008) Comparative evaluation of micro-deval abrasion test with other toughness/abrasion resistance and soundness tests. *J Mater Civ Eng* 20:343–351. [https://doi.org/10.1061/\(ASCE\)0899-1561\(2008\)20:5\(343\)](https://doi.org/10.1061/(ASCE)0899-1561(2008)20:5(343))
8. Guo Y, Markine V, Song J, Jing G (2018) Ballast degradation: Effect of particle size and shape using Los Angeles Abrasion test and image analysis. *Constr Build Mater* 169:414–424. <https://doi.org/10.1016/j.conbuildmat.2018.02.170>
9. Lane DS, Druta C, Wang L, Xue W (2011) Modified micro-deval procedure for evaluating the polishing tendency of coarse aggregates. *Transp Res Rec: J Transp Res Board* 2232:34–43. <https://doi.org/10.3141/2232-04>
10. Czinder B, Vásárhelyi B, Török Á (2021) Long-term abrasion of rocks assessed by micro-Deval tests and estimation of the abrasion process of rock types based on strength parameters. *Eng Geol* 282:105996. <https://doi.org/10.1016/j.enggeo.2021.105996>
11. Paixão A, Fortunato E (2021) Abrasion evolution of steel furnace slag aggregate for railway ballast: 3D morphology analysis of scanned particles by close-range photogrammetry. *Constr Build Mater* 267:121225. <https://doi.org/10.1016/j.conbuildmat.2020.121225>
12. Loz PHF, Angulo SC, Rebmann MS, Tutumluer E (2021) Use of a 3D structured-light scanner to determine volume, surface area, and shape of aggregates. *J Mater Civ Eng* 33:04021240. [https://doi.org/10.1061/\(ASCE\)MT.1943-5533.0003824](https://doi.org/10.1061/(ASCE)MT.1943-5533.0003824)
13. Zhihong N, Zhengyu L, Xiang W, Jian G (2018) Evaluation of granular particle roundness using digital image processing and computational geometry. *Constr Build Mater* 172:319–329. <https://doi.org/10.1016/j.conbuildmat.2018.03.246>
14. Paixão A, Resende R, Fortunato E (2018) Photogrammetry for digital reconstruction of railway ballast particles—A cost-efficient method. *Constr Build Mater* 191:963–976. <https://doi.org/10.1016/j.conbuildmat.2018.10.048>
15. AgiSoft PhotoScan (Version 1.8.6) (2022). Retrieved from <http://www.agisoft.com/downloads/installer/>
16. CloudCompare (version 2.12) [GPL software] (2022). Retrieved from <http://www.cloudcompare.org/>
17. Boltz SJ, Pey K (2008) Particle shape: A review and new methods of characterization and classification. *Sedimentology* 55:31–63. <https://doi.org/10.1111/j.1365-3091.2007.00892.x>
18. Deiros Quintanilla I, Combe G, Emeriault F, Voivret C, Ferrellec J-F (2019) X-ray CT analysis of the evolution of ballast grain morphology along a Micro-Deval test: Key role of the asperity scale. *Granul Matter* 21:30. <https://doi.org/10.1007/s10035-019-0881-y>

19. Paixão A, Afonso C, Delgado B, Fortunato E (2022) Evaluation of ballast particle degradation under micro-deval testing using photogrammetry. *Lect Notes Civ Eng* 165:113–124. [https://doi.org/10.1007/978-3-030-77234-5\\_10](https://doi.org/10.1007/978-3-030-77234-5_10)
20. Kawamoto R, Andrade J, Matsushima T (2018) A 3-D mechanics-based particle shape index for granular materials. *Mech Res Commun* 92:67–73. <https://doi.org/10.1016/j.mechrescom.2018.07.002>